# Insight into the temperature dependent properties of the ferromagnetic Kondo lattice YbNiSn

A. Generalov,[1] D. A. Sokolov,[2,3] A. Chikina,[4] Yu. Kucherenko,[5] V. N. Antonov,[5] L. V. Bekenov,[5] S. Patil,[6] A. D. Huxley,[2] J. W. Allen,[7] K. Matho,[8] K. Kummer,[9] D. V. Vyalikh,[10,11,12,*] and C. Laubschat[4]

[1]*MAX IV Laboratory, Lund University, Box 118, 22100 Lund, Sweden*
[2]*School of Physics and CSEC, University of Edinburgh, Edinburgh EH9 3FD, United Kingdom*
[3]*Max-Planck-Institut für Chemische Physik fester Stoffe, D-01187 Dresden, Germany*
[4]*Institut für Festkörperphysik, Technische Universität Dresden, D-01062 Dresden, Germany*
[5]*Institute for Metal Physics, National Academy of Science of Ukraine, UA-03142 Kiev, Ukraine*
[6]*Department of Physics, Indian Institute of Technology, Banaras Hindu University, Varanasi-225001, India*
[7]*Randall Laboratory, University of Michigan, 450 Church St., Ann Arbor, Michigan 48109-1040, USA*
[8]*Institut Néel, C.N.R.S. and Université Grenoble Alpes, BP 166, 38042 Grenoble cedex 9, France*
[9]*European Synchrotron Radiation Facility, 71 Avenue des Martyrs, Grenoble, France*
[10]*Saint Petersburg State University, Physics Department, Saint Petersburg 198504, Russia*
[11]*Donostia International Physics Center (DIPC), Departamento de Fisica de Materiales and CFM-MPC UPV/EHU, 20080 San Sebastian, Spain*
[12]*IKERBASQUE, Basque Foundation for Science, 48011 Bilbao, Spain*

(Received 23 February 2017; published 30 May 2017)

Analyzing temperature dependent photoemission (PE) data of the ferromagnetic Kondo-lattice (KL) system YbNiSn in the light of the periodic Anderson model (PAM) we show that the KL behavior is not limited to temperatures below a temperature $\overline{T}_K$, defined empirically from resistivity and specific heat measurements. As characteristic for weakly hybridized Ce and Yb systems, the PE spectra reveal a $4f$-derived Fermi level peak, which reflects contributions from the Kondo resonance and its crystal electric field (CEF) satellites. In YbNiSn this peak has an unusual temperature dependence: With decreasing temperature a steady linear increase of intensity is observed which extends over a large interval ranging from 100 K down to 1 K without showing any peculiarities in the region of $\overline{T}_K \sim T_C = 5.6$ K. In the light of the single-impurity Anderson model (SIAM) this intensity variation reflects a linear increase of $4f$ occupancy with decreasing temperature, indicating an onset of Kondo screening at temperatures above 100 K. Within the PAM this phenomenon could be described by a non-Fermi-liquid-like $T$- linear damping of the self-energy which accounts phenomenologically for the feedback from the closely spaced CEF states.

DOI: 10.1103/PhysRevB.95.184433

## I. INTRODUCTION

Intermetallic rare-earth (RE) systems based on Ce, Eu, or Yb form a prototype of strongly correlated electron systems, where the interplay between almost localized $4f$ and itinerant valence states results in a wealth of extraordinary phenomena. Among them are ultraheavy quasiparticle excitations (heavy fermions) out of Fermi-liquid (FL) or non-FL ground states that also compete with localized ground states, showing magnetic order [1,2]. At a quantum critical point (QCP), various ground states can become degenerate, which is typically achieved by applying pressure or changing the chemical composition.

In that regard, YbNiSn assumes a somewhat unique role. Already at ambient pressure and without chemical doping it shows a competition between the on-site exchange interaction that leads to formation of the Kondo lattice (KL) and the intersite exchange interaction that leads to magnetic order. As a stoichiometric material with a low level of defects, YbNiSn broadens the range of experimental techniques available for studies of the QCP, such as quantum oscillations in the electrical resistivity and magnetization but also photoemission (PE). Moreover, the KL competes in this compound with ferromagnetic (FM) order, not antiferromagnetic (AFM), as in most cases.

In this work, we focus on the $T$- dependent properties in zero magnetic field that were explored by means of electrical resistivity and specific heat measurements as well as PE spectroscopy. For simulations of the PE data, we have applied both the single-impurity Anderson model (SIAM) [3] and the periodic Anderson model (PAM). The modeling results are checked for their consistency.

The studied ternary compound YbNiSn crystallizes in the orthorhombic $\varepsilon$-TiNiSi type structure with the space group symmetry $Pnma$ (number 62). The unit cell contains four formula units. All atoms are found in layers parallel to the $xz$ plane and each layer contains all three kinds of atoms. Crystallographic studies of the compound YbNiSn were performed in Ref. [4] and yielded the unit cell parameters $a = 6.960$ Å, $b = 4.410$ Å, $c = 7.607$ Å, at room temperature. Atoms are located at the $4c$ Wyckoff positions: Yb at the (0.4897, 0.25, 0.2970), Ni at the (0.2026, 0.25, 0.5857), and Sn at the (0.8074, 0.25, 0.5866) positions. The nearest neighbor environment of the Yb atom consists of two distorted octahedra of Ni and Sn atoms, shown in Fig. 1. The interatomic distances for Yb-Ni are between 2.969 Å and 3.266 Å and for Yb-Sn between 3.068 Å and 3.182 Å. The next nearest neighbors of a Yb atom are four Yb atoms located at the vertices of a much distorted tetrahedron; two of them are at the distance of 3.552 Å (shown in the polyhedra in Fig. 1) and the other two at 3.797 Å.

*Corresponding author: Denis.Vyalikh@dipc.org

 

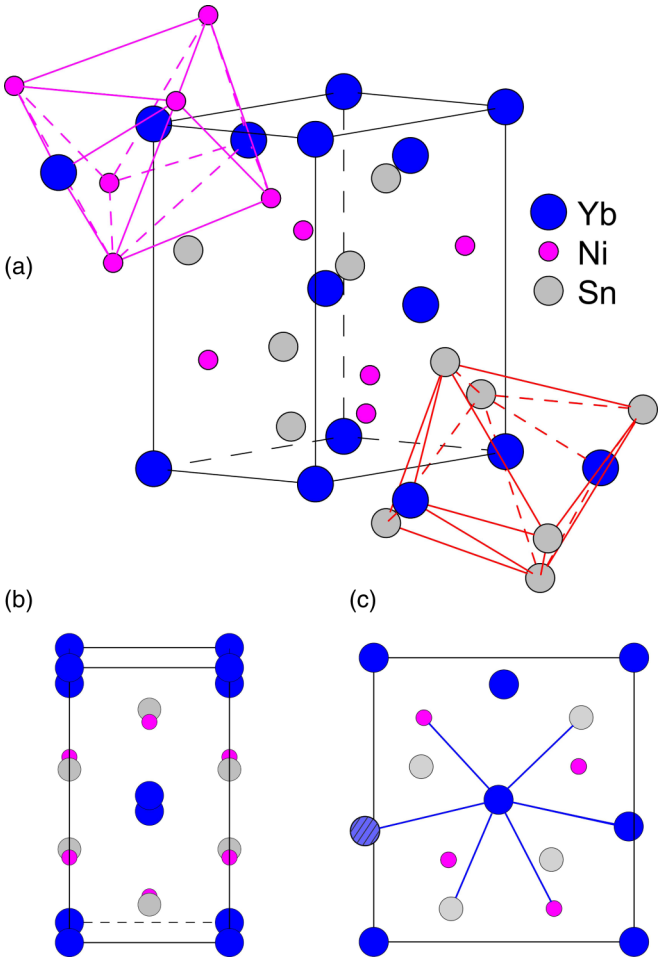


FIG. 1. (a) Schematic representation of the YbNiSn crystal structure. Note that the origin is shifted with respect to its symmetry group position to put the Yb atoms in the vertices of the unit cell for better visualization. (b) The unit cell projected on the $yz$ plane. The coordinate system is slightly rotated around the $y$ axis in order to show all atoms in the layer. (c) The unit cell projected on the $xz$ plane. The bonds of the Yb atom within the $xz$ atomic layer are shown.

## II. EXPERIMENT

Single crystals of YbNiSn were grown by melting stoichiometric amounts of the elements welded in molybdenum crucibles and annealing at 800 °C for 120 hours. Powder x-ray diffraction confirmed the absence of impurity phases. Large single crystals produced by this method showed a small mosaic of ∼0.5 degree (FWHM) measured in the cold neutron beam and residual resistivity ratio (RRR) between 40 and 100 depending on direction of current with respect to the crystallographic orientation. Heat capacity was measured using the physical property measurements system by Quantum Design. Electrical resistivity was measured using a conventional four-probe technique with a lock-in amplifier with the current parallel to the $a$ axis.

PE experiments were performed at the $1^3$-ARPES instrument of beamline UE112 PGM-2 at BESSY-II synchrotron radiation facility and at the SIS instrument of the Swiss Light Source. Both instruments are equipped with a Scienta R4000 photoelectron energy analyzer. The SIS instrument has a six-axis CARVING manipulator with high angular precision which is ideally suited for ARPES experiments down to 10 K. The $1^3$-ARPES instrument at BESSY-II allows ARPES measurements at temperatures close to 1 K with ultrahigh energy resolution. The samples were cleaved in ultrahigh vacuum and explored by photoelectron spectroscopy. The temperature-dependent measurements were performed always going from high to low temperatures in order to avoid fast sample aging.

## III. RESULTS OF RESISTIVITY AND SPECIFIC HEAT MEASUREMENTS

The electrical resistivity $\rho(T)$ along the $a$ axis in the orthorhombic crystal structure is shown in Fig. 2(a). A quantitative modeling, including strong anisotropy [4], requires an orbitally degenerate KL with exchange parameters that are orbital- and momentum-dependent. The KL model has the same relation to the PAM as the single site Kondo model to the SIAM: They are linked via the Schrieffer-Wolff transformation [5], valid when the state of Yb is almost trivalent.

The resistivity has two Kondo-like regimes, $d\rho/dT < 0$. The higher one points to the presence of Kondo screening on a $J = 7/2$ multiplet of $f$ orbitals. Because of a large spin-orbit (SO) splitting in Yb, the excited multiplet $J = 5/2$ is an example of degrees of freedom that are frozen out before any observable binding energy (BE) can be gained from the Kondo screening. In this case, perturbation theory is sufficient to define a Kondo temperature $T_K^{(8)}$ for an effective multiplicity $N_f = 2J + 1 = 8$ [5]. Whether $T_K^{(8)}$ ($k_B \equiv 1$) is the right energy scale for fluctuations within the multiplet depends further on the crystal-electric field (CEF) splittings. From inelastic neutron scattering [6], the lowest excitation is placed at ∼120 K and two additional doublets of the orthorhombic level scheme appear closely spaced. The plateau between 50 and 100 K, followed by the second regime with $d\rho/dT < 0$, are

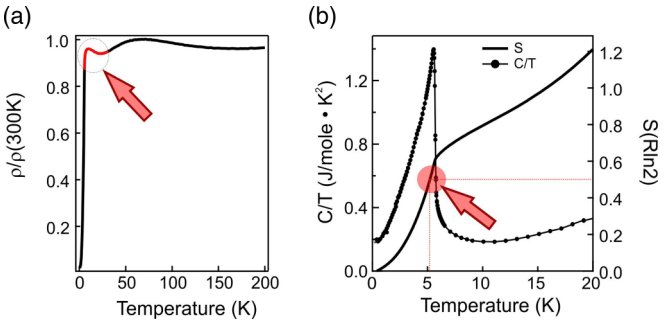


FIG. 2. Bulk properties of YbNiSn (magnetic field $\mathbf{H} = 0$): (a) $T$ dependence of the electrical resistivity along the $a$ axis. The rise below 150 K signals the Kondo screening of a $J = 7/2$ multiplet. The broad feature at ∼70 K corresponds to the freezing out of the lowest CEF excitation. The KL formation sets in below the maximum at ∼10 K (arrow). The resistivity drop is accentuated by the suppression of spin disorder scattering in the FM phase. (b) $T$ dependence of the specific heat $C/T$ and the entropy $S(T)$. The large, lambdalike anomaly at $T_C = 5.6$ K marks the FM transition. The arrow points to the fact that only half the entropy of a two level system, $S = \frac{1}{2}R\ln 2$, is recovered at $T_C$. The red dot indicates the zone of intense competition between FM order and KL formation.

nonperturbative effects, attributed to the progressive freezing of excited CEF levels and the survival of an effective Kramers doublet. As the noncrossing approximation SIAM + NCA reveals [7], the many body wave function of this ground doublet is dressed by the higher CEF orbitals, to the extent that they have contributed to the BE of the Kondo screening before being frozen out. The resistivity drop below ∼10 K is the coherent effect, captured only by a lattice model.

Specific heat and entropy measurements are shown in Fig. 2(b). The FM transition at $T_C$ is marked by the lambdalike anomaly in $C/T$. Two features below $T_C$ provide evidence that Kondo screening continues in the FM state: (i) The low-$T$ limit of $C/T$, $\gamma \sim 200$ mJ/mole K$^2$, is two orders of magnitude higher than that of an uncorrelated metal like Cu. An even higher value of ∼300 mJ/mole K$^2$ was reported previously for polycrystalline arc-molten samples [8]. This large $\gamma$ value indicates the formation of heavy quasiparticles (QP). (ii) In a localized moment system, involving only $N_f = 2$, the entropy recovered at the transition should approach $R \ln 2$, where $R$ is the gas constant. As a working definition for a QP scale $\overline{T}_K$ we take the point where $S(T) \sim \frac{1}{2} R \ln 2$ [9]. The red dot indicates that $\overline{T}_K$ is not sharply defined. The range includes $T_C = 5.6$ K but also a sharp negative peak at ∼7 K in the thermopower [6]. In the discussion of our PE simulations, the question arises whether this empirical scale can be related to the width of a QP band in the PAM, also denoted as $\overline{T}_K$ [10,11]. For the purpose of including orbital effects in the PAM, we define $\overline{T}_K^{(N_f)}$, specifying the effective degeneracy. The respective scale in the SIAM is defined without the overbar. The fact that $S(T)$ continues to rise smoothly beyond $R \ln 2$ signals again the necessity to take $N_f > 2$ into account.

## IV. RESULTS FROM PHOTOEMISSION AND DISCUSSION IN LIGHT OF ANDERSON MODELS

### A. SIAM versus PAM

The multiple competitions, seen in the bulk properties, make YbNiSn very attractive for a PE study, in order to round off recent insights gained in $YbRh_2Si_2$ and $YbIr_2Si_2$ [12–15]. Since PE covers low as well as high BE, the interpretations have to use either the SIAM or the PAM, without resorting to the Schrieffer-Wolff transformation. That one is dealing with KL physics has to be checked by the valence condition that the number of holes in the $4f$ shell is only slightly below $n_f = 1$.

The SIAM interpretation of the "Kondo peak" in angle integrated PE, particularly its $T$ dependence, has been a lively topic ever since the 1980's [16], in which SO and CEF splittings play a major role. It is instructive to briefly retrace some highlights, because they vindicate the opinion that PE is able to make contact with bulk properties. Patthey *et al.* [17] first applied SIAM + NCA to $CeSi_2$. Later, an extended and quasilinear $T$ dependence was observed in this compound [18,19] that turned out to be robust enough to survive an extrinsic convolution with a broad energy resolution function [20]. As discussed below, this may be relevant for our present observations on YbNiSn. A resonance position slightly below $E_F$, as expected for Yb, was first checked on $YbAl_3$ by L. H. Tjeng *et al.* [21], where $T$ dependence in agreement with NCA was also confirmed. Applicability to both Ce and Yb contributed essentially to the general acceptance of the SIAM picture. The progress in energy resolution enabled Reinert *et al.* [18,19] to resolve pairs of SO and CEF satellites on both sides of the Kondo resonance. The simulation of spectral weights and detailed $T$ dependence of satellite features with SIAM + NCA [7] confirms the ubiquitous presence of SO and CEF splittings.

The argument for a SIAM interpretation has always been that the angle integrated intensity is proportional to a density of states (DOS), i.e., a trace over momentum resolved intensities. The current challenge to PE is therefore to resolve features near $E_F$ that can be attributed to a QP-DOS. For example, the renormalized band theory for $YbRh_2Si_2$ [22], exhibits van Hove singularities (VHS) in the DOS that would be wiped out in the corresponding SIAM. Will it be possible for PE with extreme energy resolution to pinpoint evidence for strongly renormalized VHS? Such new challenges require a better understanding of the subtle differences between SIAM and PAM, assuming identical parameters for the $f$ shell and the hybridization. Finally, for quantitative answers, the specific energy convolutions of PE as a one-step process must also be taken into account [23].

The dynamical mean field theory (DMFT) offers a key to the general relationship and also the difference between SIAM and PAM. The SIAM provides a local "dynamical mean field" that solves a lattice self-energy (SE) for the PAM. Although this SE is "local," in the sense that it is independent of momentum, translational symmetry is recovered by using the proper Dyson equation for a lattice, which is block diagonal in the symmetry label $k$. The meaning of this label, which extends only over a single Brillouin zone (BZ), is that of crystal momentum modulo umklapp. In order to model an angle integrated PE spectrum, the partial $i$-DOS for the set of orbital characters "$i$" are needed, together with matrix elements depending on the photon energy. Intense theoretical studies exist only for the case of a Kramers doublet ($N_f = 2$) [10,24–28]. In the paramagnetic state, the problem reduces to finding the Kramers degenerate $c$-DOS and $f$-DOS, without further orbital distinction. Van Hove singularities, broadened by FL damping, are noticeable in DMFT + NRG calculations on lattices in finite dimension and at low $T$ [10,28]. To reach the limit $T \to 0$, the numerical renormalization group solution for the solver, SIAM + NRG [29], bridges certain deficiencies of SIAM + NCA. The Anderson parameters [3] assumed in these studies are generally too small ($U$) or too large ($V$) for direct application to Ce and Yb. In principle, the material specific LDA + DMFT modeling of compounds with strong correlations requires all orbitals of a partly filled $d$ or $f$ shell [30], but the actual application to RE compounds poses an extreme numerical challenge. In the pioneering work on $CeIrIn_5$ [31,32], the CEF splittings are not yet included [33].

The toy model, proposed below, is intended to provisorily fill this gap, until DMFT routines for the PAM with CEF splitting become available. It has the translationally invariant features of a PAM but introduces a simplified picture for the $f$ shell, with multiplicity $N_f$ treated as phenomenological parameter. The hierarchy of energy scales can be inferred, via the Schrieffer-Wolff transformation, from the SIAM [5]. The toy model aims to explain at least some of the remaining discrepancies in earlier interpretations for Ce [34,35] or Yb [36–38] compounds.

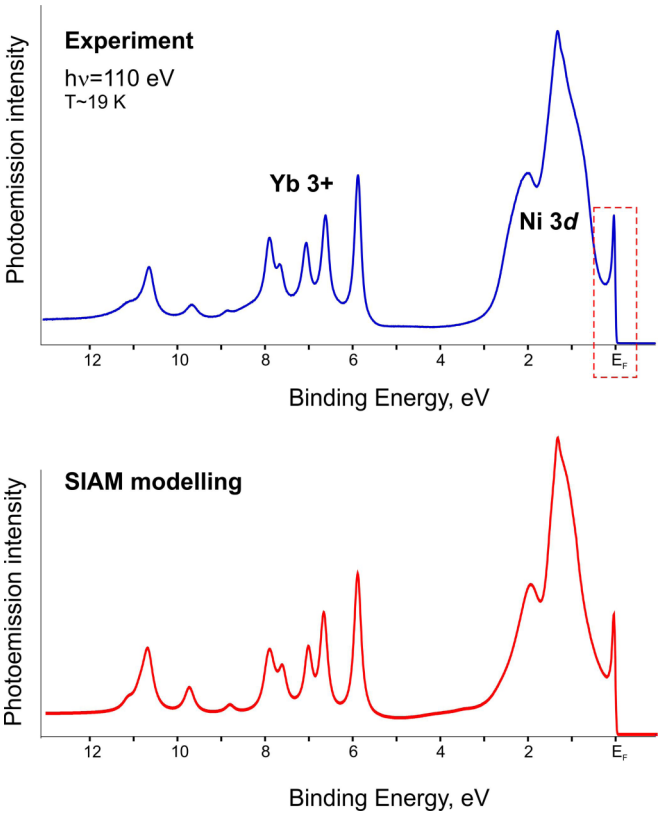


FIG. 3. PE spectrum of the YbNiSn taken at $h\nu = 110$ eV and $T = 19$ K (upper panel) and its simulation by means of the SIAM with hybridization strength $\Delta = 0.201$ eV (lower panel).

### B. Photoemission spectra and the SIAM simulation

The upper panel of Fig. 3 shows an angle integrated PE spectrum of YbNiSn, measured on a freshly cleaved sample, at photon energy $h\nu = 110$ eV, where the relative intensity of $f$ emission is large. Clearly resolved features in the spectrum are: (i) the well-known broad $4f^{12}$ final state multiplet lying at a BE between 5.9 and 11.5 eV as it is expected from photoionization of a trivalent Yb $4f^{13}$ ground-state configuration, (ii) strong emissions from the Ni $3d$ valence band (VB) between 0.3 and 3 eV BE, and (iii) a sharp peak close to $E_F$ which was not predicted in the band-structure calculations. This feature is assigned to the $4f^{13}_{7/2}$ final states arising from a $4f^{14}$ admixture to the trivalent bulk ground state. Considering the SO splitting, the related $4f^{13}_{5/2}$ component is expected at ~1.3 eV BE. Looking closely, a weak shoulder at the low-energy tail of the Ni $3d$ band could be seen and assigned to the respective state. The PE evidence for Kondo physics is the simultaneous observation of an intense $Yb^{3+}$ feature together with a sharp peak at $E_F$.

This assignment implies that the resonance at $E_F$ is not perturbed by the surface valence instability towards $Yb^{2+}$. A respective divalent surface signal is expected between 0.5 and 1.0 eV BE [13,21] and masked here by the intense Ni $3d$ emission. No measurable $T$ dependence is observed in this range, which allows us to accurately normalize the raw PE spectra to the high BE tail of Ni $3d$ [Fig. 4(a)] and attribute the $T$ dependence in the vicinity of $E_F$ only to the bulk excitations [14].

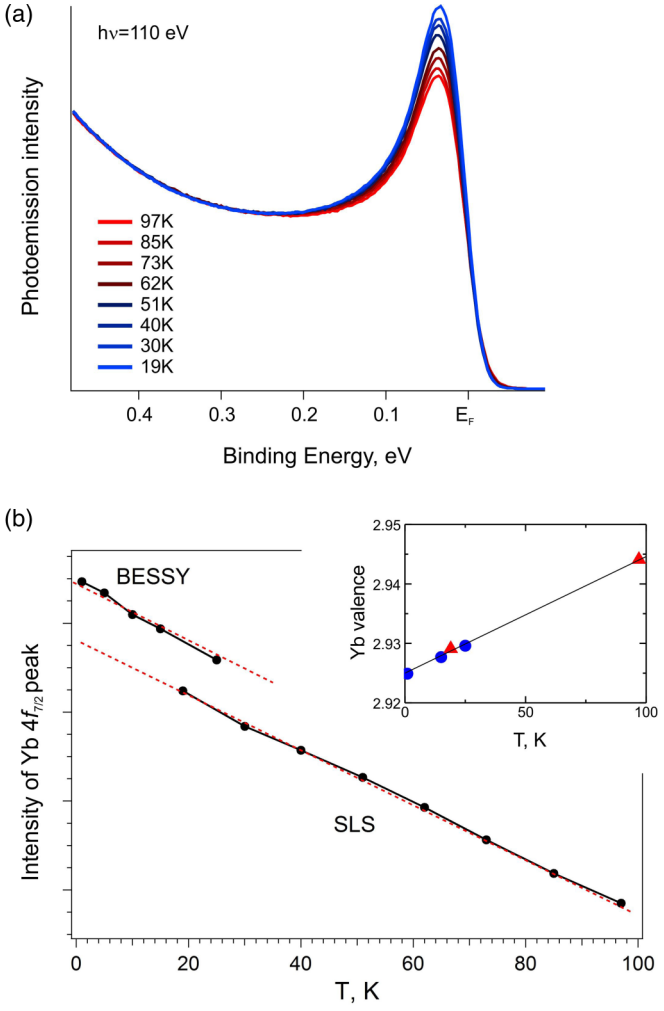


FIG. 4. (a) PE peak near $E_F$, corresponding to the $4f^{13}_{7/2}$ final-state configuration, measured from 97 K to 19 K. (b) $T$ dependence of the integrated weight for two series of measurements. Inset: $T$ dependence of the Yb valence, obtained from the SIAM simulations based on the BESSY (blue circles) and SLS (red triangles) experiments.

The SIAM modeling in the lower panel of Fig. 3 assumes an atomiclike $f$ shell ($N_f = 14$) and a realistic band-structure input. A large SO interaction of 1.28 eV splits the $4f^{13}$ final state into multiplets $J = 7/2$ and $J = 5/2$. The CEF splittings inside each multiplet are neglected. The simulation of the $T$ dependence (not shown) is phenomenological: A $T = 0$ spectrum is first obtained by the Gunnarsson-Schönhammer approach [39,40] and a hybridization strength $\Delta(T)$ is then varied to model the evolution with $T$. By retaining $N_f = 14$, a good overall fit up to the $4f^{12}$ final states is achieved. This allows us to extract reliable estimates for $U$ and $n_f$ (for details see Supplemental Material [41]).

The nominal valence $\nu = 2 + n_f(T)$, as determined for five different temperatures, is shown in the inset of Fig. 4(b), confirming near trivalent Yb. A small deviation $n_f < 1$ is already present at the highest $T$ and extends with a linear slope over at least an order of magnitude above and below the empirically defined $\overline{T}_K$.

Figure 4(a) shows the low energy part of the raw PE spectra, taken at SLS from 97 K down to 19 K. The peak intensity is

clearly below $E_F$, as expected for Yb [21]. An influence of the Fermi function is noticeable only in the tail above $E_F$. Any fine structure, due to a difference between SIAM and PAM simulation, should show up here. The absence of marked fine structure in the case of YbNiSn can have several origins. The renormalized bands that form the coherent part of the $4f^{13}_{7/2}$ final state configuration may have smaller CEF splittings than in $YbRh_2Si_2$ [22], so that they all appear bunched together under the large resonance width of ∼50 meV. This can explain the absence of separate CEF satellites but does not exclude a fine structure due to lattice effects. We argue that there is a further convolution with an intrinsic broadening function, due to the particular difficulty of cleaving YbNiSn along well defined crystallographic planes.

An exceptionally high peak intensity, in comparison with most other Yb compounds, is attributed to the low level of defects in the bulk. The surprising monotonic rise of the peak continued with decreasing $T$, as verified from 23 K to 1 K in a second experiment at BESSY-II. A typical characteristic of Kondo screening is a resonance that does not simply sharpen at constant weight. Rather, peak height and spectral weight increase together. A quantitative analysis of the weight, as obtained by integrating over the intensity, is plotted in Fig. 4(b). The spectra were normalized with respect to the VB emission for BE > 0.25 eV. The $T$ dependence of the weight has the same linear slope in both data sets and it is remarkable that there is no measurable deviation at $T_C$. The extended interval of linear $T$ dependence, correlated with the evolution of $n_f(T)$ (inset), is the central experimental result, reported here.

### C. A toy model for PAM and its results

A PAM simulation with Kramers doublets only ($N_f = 2$), using similar Anderson parameters as in the SIAM and a SE function $\Sigma_f(\omega,T)$ from DMFT [10,11,24,26,27], leads to contradictory results for the $k$-integrated spectrum near $E_F$. On the one hand, extrapolating from the literature to our scenario, at the lowest available $T$, we find $\overline{T}_K^{(2)} \sim 0.72$ meV ≡ 8.4 K for the width of the QP band, in agreement with the empirical $\overline{T}_K$ from the bulk measurements. Self consistent fillings $n_f \sim 0.9$ and $n_c \sim 0.2$ confirm an asymmetric KL scenario, with $n = n_f + n_c = 1.1$ slightly above "quarter filling," where competition with both FM and AFM order was found, depending on $U$ and $n$. A small number of holes in the VB, $n_c \to 0$, is the regime of "protracted screening" [24,35]. The main consequence for spectroscopy is a renormalized band width $\overline{T}_K^{(2)} \ll T_K^{(2)}$, strongly reduced relative to the corresponding SIAM width. On the other hand, the model with Kramers doublets only leads to a $T$ dependence of the calculated QP band that disagrees strongly with experiment. The integrated weight drops initially $\propto(T/\overline{T}_K)^2$, followed asymptotically by log-linear decay.

In our interpretation, both the large width of the PE resonance and the extended interval of linear $T$ dependence have a common origin in the effect of a set of closely spaced, already hybridized bands, resulting from the orbital degrees of freedom in the presence of rather weak CEF splittings. This implies that Kondo screening begins far above the empirical $\overline{T}_K$, a reasoning supported by the CEF effects in the SIAM.

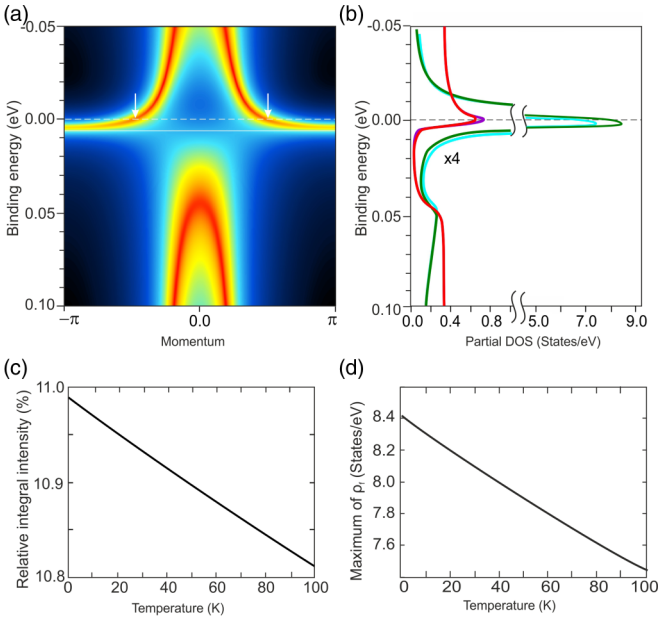


FIG. 5. Fine structure around $E_F$, as simulated by the toy model. The half width of the bare VB is $W = 1$ eV. The effective KL scale is $k_B\overline{T}_K^{(8)} = 5.3$ meV. (a) $k$-resolved $f$ intensity at $T = 0$, showing a QP band and a less renormalized bonding band, both of finite width, repelling each other at the renormalized $f$ level $\epsilon_f^*$ (continuous line). The crossing points (arrows) lie on the large FS. (b) Partial DOS $\rho_f(\epsilon)$ (green line) and $\rho_c(\epsilon)$ (red line), at $T = 0$ K and 100 K. The $f$-DOS dominates in an interval of ±10 meV around $E_F$ and again around the top of the bonding band. Simulated $T$ dependences: (c) Weight of $\rho_f(\epsilon)$ (integrated over ±0.1 eV) as a percentage of the Pauli weight and (d) maximum of $\rho_f$.

A large Fermi surface (FS), present already at 100 K [15], also fits into this picture and definitely demands a lattice model for its interpretation.

Our toy model is defined on the $k$-resolved level by a phenomenological replacement $\Sigma_f(\omega,T) \to \Sigma_{\rm eff}(\omega,T) = \Sigma_{\rm CFM}(\omega) + i\tilde{\Sigma}''(T)$ of the SE from DMFT, otherwise keeping the same 2×2 Dyson equation [11]. The first term is obtained with the continued fraction method (CFM) [42,43]. The width of the four overlapping QP bands is increased to an effective KL scale $\overline{T}_K^{(8)}$. The CFM incorporates the Hubbard sum rules and the Luttinger sum rule, with FS volume $n/2$. Here, $n$ is kept constant as a function of $T$ by self consistently varying the position of $\epsilon_c$ [24]. The self-consistency generates an implicit $T$ dependence in $\Sigma_{\rm CFM}(\omega)$. The $\omega$-independent broadening $\tilde{\Sigma}''(T)$ replaces $\Delta(T)$ in the SIAM simulation as fitting parameter. It has a more direct physical interpretation, since it models the uncertainty in the relative position of the four bands as a life time effect on the $k$-resolved level [44].

Results for the toy model, with Anderson parameters for an asymmetric KL scenario (see Supplemental Material [41]), are shown in Fig. 5. The effective damping rate, extracted from the measured $T$ dependence in Fig. 4(b), is of a non-FL type: $\tilde{\Sigma}_f''(T) = A + BT$, with a $T = 0$ offset $A \sim 2\overline{T}_K^{(8)}$ and a linear thermal slope $B = 0.6$.

The $k$-resolved plot of $f$ intensity at $T = 0$, [Fig. 5(a)], shows a QP band and an antibonding band, both strongly

renormalized and blurred by the anomalous damping. The $f$ intensity is high above and below the renormalized $f$ level $\epsilon_f^*$. For the definition of the FS, it is important that the term $\tilde{\Sigma}_{\mathrm{CFM}}(\omega)$, in the absence of the phenomenological changes, can be mapped exactly on the DMFT + NRG solution in the limit $T \to 0$, which has a discontinuity in the momentum distribution at $k_F$. This was checked by benchmarking with scenarios near quarter filling for $U = 3.5W$ and $U = 10W$ [10]. In the presence of $\tilde{\Sigma}_f''(0)$, the discontinuity is wiped out but a FS remains defined in ARPES by the $k$ values where the intensity peaks at zero BE [15]. The partial $f$-DOS $\rho_f(\epsilon)$ and valence band $c$-DOS $\rho_c(\epsilon)$ in Fig. 5(b) both show resonant behavior. The highest peak is near the bottom of the QP band. The linear $T$ dependence of both the weight and the peak height [Figs. 5(c) and 5(d)], in agreement with Fig. 4, is explained by a $T$- linear damping inside the SE, on the $k$-resolved level.

Note that $\epsilon_f^*$ is the center of gravity of the total split resonance. Here, its position close to the main peak is a signature of the asymmetric KL. The QP DOS alone, of width $\overline{T}_K^{(8)}$, does not correspond to the Kondo peak in the SIAM. When the split resonance is measured with insufficient resolution, the "Kondo peak" reappearing at $\epsilon_f^*$ includes both sides. We identify the overall width with the scale $T_K^{(8)}$ of the SIAM. The pseudogap can be wiped out intrinsically when the spacings between the CEF levels increase. For large spacings, each SO or CEF satellite is expected to be modified by a lattice signature. The $T$ dependence of the resonance weight is observable even with moderate resolution. A hierarchy of the various characteristic scales, evaluated for the case of YbNiSn, is presented in the Supplemental Material [41].

## V. SUMMARY

In conclusion, PE spectra of the Kondo lattice compound YbNiSn reveal an unusual $T$ dependence of the Fermi-level peak, which includes contributions from the QP resonance and its unresolved CEF satellites. With decreasing temperature, the peak reveals a steady linear increase of intensity which extends over a large temperature range from 100 K to 1 K, without showing any peculiarities in the region of $\overline{T}_K \sim T_C$.

In the light of the SIAM, these intensity variations reflect a linear increase of $4f$ occupancy, indicating an onset of the Kondo lattice behavior at temperatures above 100 K. Within the PAM this phenomenon could be described by a non-Fermi-liquid-like $T$-linear damping in the self-energy which accounts phenomenologically for the feedback from closely spaced CEF-split bands. Given this interpretation, use of the "non-FL" terminology has to be taken with a grain of salt. In particular, we do not have enough evidence to ascribe the $T$-linear damping to the presence of a QCP at $T = 0$.

When combined with the large, $T$-invariant FS in $YbRh_2Si_2$ [15], our findings on the resonance near $E_F$ in the PE spectrum of YbNiSn confirm that the formation of a coherent state at ~10 K, as visible in the transport, has to be dissociated from the formation of renormalized bands and the beginning of Kondo screening at much higher $T$.

## ACKNOWLEDGMENTS

This work was supported by the German Research Foundation (DFG; Grants No. VY64/1-3, No. GE602/2-1, No. GRK1621, and SFB1143) and by Research Grant No. 15.61.202.2015 of Saint Petersburg State University. D.A.S. and A.D.H. acknowledge support from EPSRC Grant No. EP/J00099X/1. The authors would like to acknowledge Christoph Geibel for stimulating discussions and valuable suggestions.

[1] P. Gegenwart, Q. Si, and F. Steglich, Nat. Phys. **4**, 186 (2008).
[2] P. Coleman, in *Handbook of Magnetism and Advanced Magnetic Materials* (John Wiley and Sons, Chichester, UK, 2007), Vol. 1, pp. 95–148.
[3] P. W. Anderson, Phys. Rev. **124**, 41 (1961).
[4] P. Bonville, P. Bellot, J. A. Hodges, P. Imbert, G. Jéhanno, G. Le Bras, J. Hammann, L. Leylekian, G. Chevrier, P. Thuéry, L. D'Onofrio, A. Hamzic, and A. Barthélémy, Physica B **182**, 105 (1992).
[5] B. Cornut and B. Coqblin, Phys. Rev. B **5**, 4541 (1972).
[6] D. T. Adroja, B. D. Rainford, and T. Takabatake, Physica B **253**, 269 (1998).
[7] J. Kroha, S. Kirchner, G. Sellier, P. Wölfle, D. Ehm, F. Reinert, S. Hüfner, and C. Geibel, Physica E (Amsterdam) **18**, 69 (2003).
[8] M. Kasaya, T. Tani, K. Kawate, T. Mizushima, Y. Isikawa, and K. Sato, J. Phys. Soc. Jpn. **60**, 3145 (1991).
[9] C. Klingner, C. Krellner, M. Brando, C. Geibel, F. Steglich, D. V. Vyalikh, K. Kummer, S. Danzenbächer, S. L. Molodtsov, C. Laubschat, T. Kinoshita, Y. Kato, and T. Muro, Phys. Rev. B **83**, 144405 (2011).
[10] A. Benlagra, Th. Pruschke, and M. Vojta, Phys. Rev. B **84**, 195141 (2011).
[11] Our notations for the PAM are as in Ref. [10].
[12] D. V. Vyalikh, S. Danzenbächer, Y. Kucherenko, K. Kummer, C. Krellner, C. Geibel, M. G. Holder, T. K. Kim, C. Laubschat, M. Shi, L. Patthey, R. Follath, and S. L. Molodtsov, Phys. Rev. Lett. **105**, 237601 (2010).
[13] K. Kummer, Y. Kucherenko, S. Danzenbächer, C. Krellner, C. Geibel, M. G. Holder, L. V. Bekenov, T. Muro, Y. Kato, T. Kinoshita, S. Huotari, L. Simonelli, S. L. Molodtsov, C. Laubschat, and D. V. Vyalikh, Phys. Rev. B **84**, 245114 (2011).
[14] S. Patil, K. Kummer, A. Hannaske, C. Krellner, M. Kuhnt, S. Danzenbächer, C. Laubschat, C. Geibel, and D. Vyalikh, JPS Conf. Proc. **3**, 011001 (2014).
[15] K. Kummer, S. Patil, A. Chikina, M. Güttler, M. Höppner, A. Generalov, S. Danzenbächer, S. Seiro, A. Hannaske, C. Krellner, Yu. Kucherenko, M. Shi, M. Radovic, E. Rienks, G. Zwicknagl, K. Matho, J. W. Allen, C. Laubschat, C. Geibel, and D. V. Vyalikh, Phys. Rev. X **5**, 011028 (2015).
[16] J. W. Allen, S. J. Oh, O. Gunnarsson, K. Schönhammer, M. B. Maple, M. S. Torikachvili, and I. Lindau, Adv. Phys. **35**, 275 (1986); J. W. Allen, J. Phys. Soc. Jpn. **74**, 34 (2005).
[17] F. Patthey, W.-D. Schneider, Y. Baer, and B. Delley, Phys. Rev. Lett. **58**, 2810 (1987).

[18] F. Reinert, D. Ehm, S. Schmidt, G. Nicolay, S. Hüfner, J. Kroha, O. Trovarelli, and C. Geibel, Phys. Rev. Lett. **87**, 106401 (2001).
[19] D. Ehm, S. Hüfner, F. Reinert, J. Kroha, P. Wölfle, O. Stockert, C. Geibel, and H. v. Löhneysen, Phys. Rev. B **76**, 045117 (2007).
[20] See the three panels of Fig. 9 in Ref. [19].
[21] L. H. Tjeng, S.-J. Oh, E.-J. Cho, H.-J. Lin, C. T. Chen, G.-H. Gweon, J.-H. Park, J. W. Allen, T. Suzuki, M. S. Makivić, and D. L. Cox, Phys. Rev. Lett. **71**, 1419 (1993).
[22] G. Zwicknagl, J. Phys.: Condens. Matter **23**, 094215 (2011); see the RB result for $H = 0$ in Fig. 3.
[23] R. O. Kuzian and E. E. Krasovskii, Phys. Rev. B **94**, 115119 (2016).
[24] A. N. Tahvildar-Zadeh, M. Jarrell, and J. K. Freericks, Phys. Rev. Lett. **80**, 5168 (1998).
[25] Th. Pruschke, R. Bulla, and M. Jarrell, Phys. Rev. B **61**, 12799 (2000).
[26] D. Meyer and W. Nolting, Phys. Rev. B **62**, 5657 (2000).
[27] A. Amaricci, L. de′ Medici, G. Sordi, M. J. Rozenberg, and M. Capone, Phys. Rev. B **85**, 235110 (2012).
[28] A. Kainz, A. Toschi, R. Peters, and K. Held, Phys. Rev. B **86**, 195110 (2012).
[29] T. A. Costi, J. Kroha, and P. Wölfle, Phys. Rev. B **53**, 1850 (1996).
[30] A. Georges, L. De Medicis, and J. Mravlje, Annu. Rev. Condens. Matter Phys. **4**, 137 (2013).
[31] J. H. Shim, K. Haule, and G. Kotliar, Science **318**, 1615 (2007).
[32] H. C. Choi, B. I. Min, J. H. Shim, K. Haule, and G. Kotliar, Phys. Rev. Lett. **108**, 016402 (2012).
[33] J. H. Shim (private communication)
[34] J. J. Joyce, A. J. Arko, J. Lawrence, P. C. Canfield, Z. Fisk, R. J. Bartlett, and J. D. Thompson, Phys. Rev. Lett. **68**, 236 (1992).
[35] A. J. Arko, J. J. Joyce, L. E. Cox, L. Morales, J. Sarrao, J. L. Smith, Z. Fisk, A. Menovsky, A. Tahvildar-Zadeh, and M. Jarrell, J. Alloys Compd. **271–273**, 826 (1998).
[36] J. M. Lawrence, A. J. Arko, J. J. Joyce, P. C. Canfield, Z. Fisk, J. D. Thompson, and R. J. Bartlett, J. Magn. Mag. Mater. **108**, 215 (1992).
[37] P. Weibel, M. Grioni, D. Malterre, B. Dardel, Y. Baer, and M. J. Besnus, Z. Phys. B **91**, 337 (1993).
[38] R. I. R. Blyth, J. J. Joyce, A. J. Arko, P. C. Canfield, A. B. Andrews, Z. Fisk, J. D. Thompson, R. J. Bartlett, P. Riseborough, J. Tang, and J. M. Lawrence, Phys. Rev. B **48**, 9497 (1993).
[39] O. Gunnarsson and K. Schönhammer, Phys. Rev. B **31**, 4815 (1985).
[40] R. Hayn, Yu. Kucherenko, J. J. Hinarejos, S. L. Molodtsov, and C. Laubschat, Phys. Rev. B **64**, 115106 (2001).
[41] See Supplemental Material at http://link.aps.org/supplemental/10.1103/PhysRevB.95.184433 for the theoretical modeling.
[42] R. Hayn, P. Lombardo, and K. Matho, Phys. Rev. B **74**, 205124 (2006).
[43] A. Chikina, PhD. thesis, TU Dresden (2016), http://katalogbeta.slub-dresden.de/id/0018051591/.
[44] N. V. Smith, P. Thiry, and Y. Petroff, Phys. Rev. B **47**, 15476 (1993).